UKAEA-CCFE-PR(23)180

L-H transition studies in recent Tritium and Deuterium-Tritium campaigns at JET

E.R. Solano, G. Birkenmeier, C. Silva, E. Delabie, J.C. Hillesheim, A. Baciero, I. Balboa, M. Baruzzo, A. Boboc, M. Brix, C. Bourdelle, I.S. Carvalho, P. Carvalho, C.D. Challis, M. Chernyshova, A. Chomiczewska, R. Coelho, T. Craciunescu, E. de la Cal, E. de la Luna, R. Dumont, P. Dumortier, M. Fontana, J.M. Fontdecaba, L. Frassinetti, D. Gallart, J. Garcia, C. Giroud, W. Gromelski, R.B. Henriques, J. Hall, A. Ho, L. Horvath, P. Jacquet, I. Jepu, E. Joffrin, A. Kappatou, P. Carvalho, D. Keeling, D. King, E. Kowalska-Strzęciwilk, M. Lennholm, E. Lerche, E. Litherland-Smith, V.G. Kiptily, K.K. Kirov, A. Loarte, B. Lomanowski, C.F. Maggi, J. Mailloux, M.J. Mantsinen, M. Maslov, A.G. Meigs, I. Monakhov, R.B. Morales, A.H. Nielsen, D. Nina, C. Noble, E. Pawelec, M. Poradzinski, G. Pucella, P. Puglia, D. Réfy, J.J. Rasmussen, E. Righi-Steele, F.G. Rimini, T. Robinson, M. Sertoli, S.A. Silburn, P. Sirén, Ž. Štancar, H.J. Sun, G. Szepesi, D. Taylor, B. Thomas, E. Tholerus, G. Verdoolaege, P. Vincenzi, B. Viola, N. Vianello, T. Wilson

L-H transition studies in recent Tritium and Deuterium-Tritium campaigns at JET

E.R. Solano, G. Birkenmeier, C. Silva, E. Delabie, J.C. Hillesheim, A. Baciero, I. Balboa, M. Baruzzo, A. Boboc, M. Brix, C. Bourdelle, I.S. Carvalho, P. Carvalho, C.D. Challis, M. Chernyshova, A. Chomiczewska, R. Coelho, T. Craciunescu, E. de la Cal, E. de la Luna, R. Dumont, P. Dumortier, M. Fontana, J.M. Fontdecaba, L. Frassinetti, D. Gallart, J. Garcia, C. Giroud, W. Gromelski, R.B. Henriques, J. Hall, A. Ho, L. Horvath, P. Jacquet, I. Jepu, E. Joffrin, A. Kappatou, P.J. Lomas, D.L. Keeling, D.B. King, E. Kowalska-Strzęciwilk, M. Lennholm, E. Lerche, E. Litherland-Smith, V.G. Kiptily, K.K. Kirov, A. Loarte, B. Lomanowski, C.F. Maggi, J. Mailloux, M.J. Mantsinen, M. Maslov, A.G. Meigs, I. Monakhov, R.B. Morales, A.H. Nielsen, D. Nina, C. Noble, E. Pawelec, M. Poradzinski, G. Pucella, P. Puglia, D. Réfy, J.J. Rasmussen, E. Righi-Steele, F.G. Rimini, T. Robinson, M. Sertoli, S.A. Silburn, P. Sirén, Ž. Štancar, H.J. Sun, G. Szepesi, D. Taylor, B. Thomas, E. Tholerus, G. Verdoolaege, P. Vincenzi, B. Viola, N. Vianello, T. Wilson

L-H transition studies in Tritium and Deuterium-Tritium campaigns at JET with Be wall and W divertor

E.R. Solano[1], G. Birkenmeier[2,3], C. Silva[4], E. Delabie[5], J.C. Hillesheim[6], A. Baciero[1], I. Balboa[6], M. Baruzzo[7], A. Boboc[6], M. Brix[6], J. Bernardo[6], C. Bourdelle[8], I.S. Carvalho[4,6,9], P. Carvalho[4,6], C.D. Challis[6], M. Chernyshova[10], A. Chomiczewska[10], R. Coelho[4], I. Coffey[6], T. Craciunescu[11], E. de la Cal[1], E. de la Luna[1], R. Dumont[8], P. Dumortier[12], M. Fontana[6], J.M. Fontdecaba[1], L. Frassinetti[13], D. Gallart[14], J. Garcia[8], C. Giroud[6], W. Gromelski[10], R.B. Henriques[4], J. Hall[15], A. Ho[16], L. D. Horton[6], L. Horvath[6], P. Jacquet[6], I. Jepu[11], E. Joffrin[8], A. Kappatou[3], D.L. Keeling[6], D.B. King[6], V.G. Kiptily[6], K.K. Kirov[6], D. Kos[6], E. Kowalska-Strzęciwilk[10], M. Lennholm[6,17], E. Lerche[12], E. Litherland-Smith[6], A. Loarte[9], B. Lomanowski[5], P.J. Lomas[6], C.F. Maggi[6], J. Mailloux[6], M.J. Mantsinen[18], M. Maslov[6], A.G. Meigs[6], I. Monakhov[6], R.B. Morales[6], A.H. Nielsen[19], D. Nina[4], C. Noble[6], E. Pawelec[20], M. Poradzinski[6], G. Pucella[21], P. Puglia[6], D. Réfy[22], J.J. Rasmussen[19], E. Righi[17], F.G. Rimini[6], T. Robinson[6], M. Sertoli[6], S.A. Silburn[6], G. Sips[17], P. Sirén[6], Ž. Štancar[23,6], H.J. Sun[6], G. Szepesi[6], D. Taylor[6], E. Tholerus[6], B. Thomas[6], G. Verdoolaege[15], P. Vincenzi[7,24], B. Viola[6], N. Vianello[7,24], T. Wilson[6] and JET contributors[*]

[1]Laboratorio Nacional de Fusión, CIEMAT, Madrid, Spain
[2]Physik-Department E28, Technische Universität München, 85748 Garching, Germany
[3]Max-Planck-Institut für Plasmaphysik, D-85748 Garching, Germany
[4]Instituto de Plasmas e Fusão Nuclear, Instituto Superior Técnico, Universidade de Lisboa, 1049-001 Lisboa, Portugal
[5]Oak Ridge National Laboratory, Oak Ridge, TN 37831, TN, United States of America
[6]UKAEA, Culham Science Centre, Abingdon, OX14 3DB, UK
[7]Consorzio RFX (CNR, ENEA, INFN, Università di Padova, Acciaierie Venete SpA) Corso Stati Uniti 4 - 35127 Padova, Italy
[8]CEA, IRFM, F-13108 Saint Paul Lez Durance, France
[9]ITER Organization, Route de Vinon-sur-Verdon, CS 90 046, 13067 Saint Paul Lez Durance Cedex, France
[10]Institute of Plasma Physics and Laser Microfusion, Hery 23, 01-497 Warsaw, Poland
[11]The National Institute for Laser, Plasma and Radiation Physics, Magurele-Bucharest, Romania
[12]Laboratory for Plasma Physics LPP-ERM/KMS, B-1000 Brussels, Belgium
[13]Fusion Plasma Physics, EECS, KTH Royal Institute of Technology, SE-10044 Stockholm, Sweden
[14]Barcelona Supercomputing Center, Barcelona, Spain
[15]Department of Applied Physics, Ghent University, 9000 Ghent, Belgium
[16]FOM Institute DIFFER, Eindhoven, The Netherlands
[17]European Commission, B-1049 Brussels, Belgium
[18]ICREA and Barcelona Supercomputing Center, Barcelona, Spain
[19]Department of Physics, Technical University of Denmark, Bldg 309, DK-2800 Kgs Lyngby, Denmark
[20]Institute of Physics, Opole University, Oleska 48, 45-052 Opole, Poland
[21]ENEA, Nuclear Fusion and Safety Department, C.R. Frascati, Via E. Fermi 45, 00044 Frascati, Italy
[22]Centre for Energy Research, POB 49, H-1525 Budapest, Hungary
[23]Slovenian Fusion Association (SFA), Jozef Stefan Institute, Jamova 39, SI-1000 Ljubljana, Slovenia
[24]Institute for Plasma Science and Technology, CNR, Padova, Italy

*See J. Mailloux et al., Nucl. Fusion 62, 042026 (2022) for affiliations.

E-mail: emilia.solano@ciemat.es

Abstract

The recent Deuterium-Tritium campaign in JET-ILW (DTE2) has provided a unique opportunity to study the isotope dependence of the L-H power threshold in an ITER-like wall environment. Here we present results from dedicated L-H transition experiments at JET-ILW, documenting the power threshold in Tritium and Deuterium-Tritium plasmas, comparing them with the matching Deuterium and Hydrogen datasets.

From earlier experiments in JET-ILW it is known that as plasma isotopic composition changes from deuterium, through varying deuterium/hydrogen concentrations, to pure hydrogen, the value of the line averaged density at which the threshold is minimum, $\bar{n}_{e,min}$, increases, leading us to expect that $\bar{n}_{e,min}(\text{T}) < \bar{n}_{e,min}(\text{DT}) < \bar{n}_{e,min}(\text{D}) < \bar{n}_{e,min}(\text{H})$. The new power threshold data confirms these expectations in most cases, with the corresponding ordering of the minimum power thresholds.

We present a comparison of this data to power threshold scalings, used for extrapolation to future devices such as ITER and DEMO.

Keywords: L-H transition, power threshold, tokamaks, Tritium, DT, JET-ILW

1. Introduction

The H-mode was 1st reported in 1982 [1]: when plasma heating exceeds a certain threshold a spontaneous transition to an improved confinement state takes place in the plasma, turbulence is reduced and a transport barrier forms at the plasma edge. H-mode is now the most common operating regime in tokamaks, and the associated improvement in confinement in the form of a pedestal for density and temperature makes it the chosen operating regime in future tokamak fusion experiments. Ensuring access to the good confinement associated to the H-mode is essential for ITER success, and so it is important to document and understand the isotopic dependence of the L-H power threshold.

A 1989 review of the ASDEX H-mode already indicated that Hydrogen (H, Protium) plasmas have higher L-H threshold (P_{LH}) power than Hydrogen-Deuterium mixtures [2]. The power threshold of hydrogenic isotopes including Tritium was studied in the 1997 D-T campaign at JET [3], leading to the conclusion that P_{LH} in hydrogenic plasmas is proportional to $2/A_{eff}$, where A_{eff} is the effective isotopic mass.

More recent JET-ILW results have shown that not only do H plasmas in general have a higher P_{LH} than Deuterium (D) plasmas, but there is a clear shift in the density at which the power threshold exhibits a minimum ($\bar{n}_{e,min}$) to higher densities for H relative to D [4],[5][6][8][9]. Additionally, for fixed toroidal field, B_{tor}, the L-H transition power threshold (P_{LH}) and $\bar{n}_{e,min}$ at JET-ILW have been shown to sensitively depend on plasma and divertor configuration, plasma current (I_p) and wall material [6], [4]. For the isotope study presented here all plasmas have the same shape, with lower X-point and ion grad-B drift towards the X-point (see Fig. 3), usually named Horizontal Target or V/H (because the inner strike is on a vertical tile and the outer on a tilted, almost horizontal, tile).

Initial studies [7], [10], [11] revealed that in Tritium L-H transitions can take place without auxiliary heating. Ohmic H-modes were first documented in D in DIII-D [12],[13], and subsequently reported in various other tokamaks (AUG [14], TUMAN-3[15], ALCATOR C-MOD [16], HT-6M [17], and Compass [18]. They were expected and observed in T plasmas at JET in the recent campaigns.

In this manuscript, as is conventional [19], [20], the power threshold P_{LH} is characterized either by $P_{loss} = P_{Ohm} + P_{Aux} + P_{fus} - dW_{dia}/dt$ or by $P_{sep} = P_{loss} - P_{rad,bulk}$. P_{Aux} is the auxiliary heating power absorbed by the plasma, P_{Ohm} the ohmic power, P_{fus} (which we took the liberty of adding to the conventional equation) is the power produced by fusion reactions and absorbed by the plasma, W_{dia} is the plasma diamagnetic energy, dW_{dia}/dt its time variation due to power

ramps or steps, and $P_{rad,bulk}$ is the radiation from the plasma core, inside the 0.95 normalised poloidal flux surface.

After many years, the 2008 multi-device ITPA L-H transition power threshold scaling [21] remains the standard against which L-H transition power threshold measurements are compared. It can be written as

$$P_{ITPA} = (0.0488 \pm 0.006)\ \bar{n}_{e20}^{0.717 \pm 0.035}\ B_{tor}^{0.803 \pm 0.032}\ S^{0.941 \pm 0.019} \quad (1)$$

with $\bar{n}_{e20}$ the line averaged density in units of 10^{20}m^{-3}, B_{tor} the toroidal magnetic field in Tesla and S the plasma surface area in m². Since that scaling was obtained dominantly with D plasmas, it is typical to multiply the formula above by $(2/A_{eff})$: that is the isotope-adjusted 2008 ITPA power threshold scaling. The 2008 ITPA multi-machine power threshold scaling was derived from L-H P_{loss} data from points with density above $\bar{n}_{e,min}$, in the so-called "high density branch", largely from experiments in C-wall machines, at low values of P_{rad}/P_{loss}, and largely in D plasmas.

A reduction of ~30% in the measured power threshold of Carbon wall tokamaks compared to metal-wall devices has been reported in AUG [23] and JET [4]. This observation led to an effort to select data only from metal wall devices to quantify P_{LH}. For JET-ILW new scalings were derived [22] and published [7]. Since they are derived from ITPA Task TC-26, they are named TC26. There are 3 versions: one for Horizontal Target plasmas, one for both Corner and Vertical Target plasmas, and one that represents both datasets with the same B_{tor} and n_{e20} dependency, but a scale factor of order 2 to fit the higher threshold of Corner and Vertical Target plasmas.

As our experiments in T and DT were all in Horizontal Target configuration, here we quote only the corresponding JET-ILW TC-26 Horizontal Target scaling:

$$P_{TC26} = (0.057 \pm 0.012)\ \bar{n}_{e20}^{1.43 \pm 0.10}\ B_{tor}^{0.77 \pm 0.015}\ S^1, \quad (2)$$

which displays a much stronger density exponent than the 2008 ITPA scaling. In this manuscript we compare our data to both these scalings (1) and (2). We shall see that high P_{rad} is unavoidable in many plasmas in JET, and in consequence we will compare both P_{loss} and P_{sep} with the ITPA scaling, following the lead of the ITER team [24], assuming low P_{rad} is to be expected in ITER.

We don't include in this manuscript an extensive review of earlier L-H transition studies from JET-C or other devices, in the understanding that it is more useful for the community that we publish the JET-ILW power threshold results as soon as possible and release the data into the ITPA threshold database, rather than wait for the outcome of detailed physics studies.
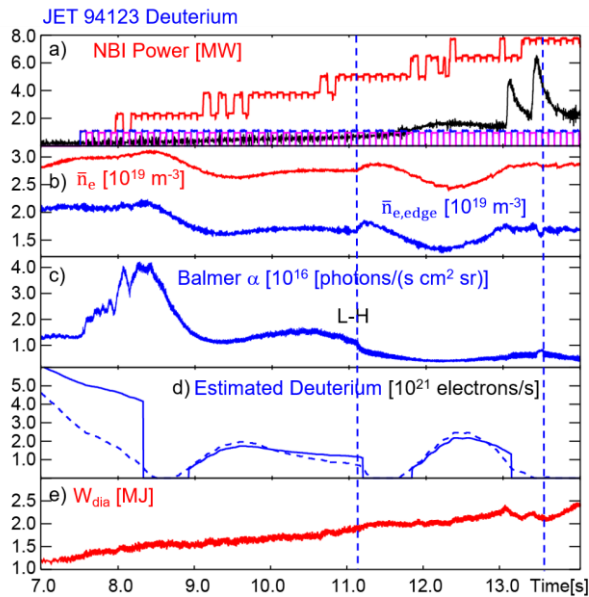
Fig. 1: Time traces of L-H transition Deuterium plasma with D-NBI heating, JET #94123. Black vertical dashed lines mark the L-H transitions at $t_{LH}=11.10s$ and 13.5s. a) total NBI injected power in red, power from core CX PINI in blue and from compensating PINI in magenta, radiated power inside 0.95 in black (both in D). b) line averaged electron density; c) Balmer alpha light from the inner divertor; d) Estimates of gas injected; e) plasma diamagnetic energy

Fig. 2: Time traces of L-H transition DT plasma with D and T-NBI heating, JET #99474 at $t_{LH}=11.36$ and $t_{LH}=17.41s$. Black vertical dashed lines mark the L-H transitions. a) total NBI injected power in red, power from D PINIs in Blue, T PINIs in magenta, radiated power inside 0.95 in black. b) densities; c) Balmer alpha light from the inner divertor; d) D(blue) and T(magenta) approximate gas injected (left axis) and Tritium concentration in black (rhs axis); e) plasma diamagnetic energy

This article is organised as follows: in section 2 we discuss experimental constraints imposed by Tritium operation and by the diagnostics available at JET, and experiment design. In Section 3 we present the power threshold as a function of density and isotope for 3 different choices of B_{tor} and I_p, discussing some interesting datapoints in some detail. In Section 4 we compare the high density branch data to the scalings. In section 5 we summarise our observations and discuss implications for future work.

2. Tritium constraints, experiment design

Operation in Tritium has many technical implications [25], quite a few of which impact experiment design. Most importantly, the JET Safety Case limits the amount of Tritium that can be injected (both via gas injection and with Neutral Beam Injection, NBI) on any given experimental day to 11 g. Stringent Tritium and neutron budgets, estimation and accounting procedures had to be followed. The number of pulses and amount of Tritium available for each experiment had to be minimised.

The main chamber Tritium Gas Injection Modules (TIMs) [26] are located next to the horizontal bolometer array and therefore interfere with tomographic reconstruction. Since the measurement of bulk radiation is important to characterise P_{LH}, we only used divertor TIMs in L-H experiments.
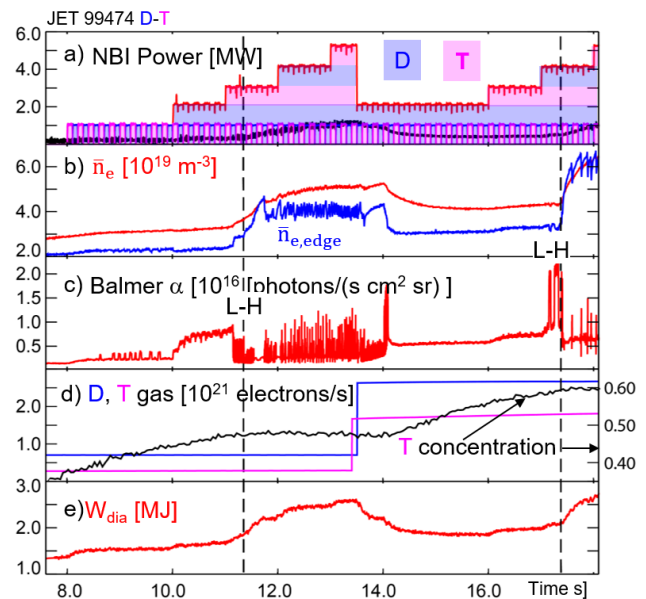
Deuterium Gas Injection Modules (GIMs) that do not interfere with bolometry were available both in divertor and main chamber, facilitating both D and DT experiments. Since we had already established in D plasmas that the choice of GIMs (whether located in main chamber or divertor) doesn't affect the power threshold, we were able to carry out experiments despite occasional issues with specific GIMs or TIMs: we simply switched to another suitable one.

Concentrations of H, D, T were measured in the sub-divertor region with a Penning gage [27], and with the Balmer alpha line ratios measured with a high resolution spectrometer with viewing cords looking into the inner and outer divertor regions. Both measurements of concentration typically agree to within 5%.

In this paper we define as H plasmas those with H concentration $c_H=n_H/(n_H+n_D+n_T)$ greater than 0.97, Deuterium as those with $c_D>0.95$, Tritium those with $c_T>0.95$, but we included also some ohmic T transitions with c_T between 0.9 and 0.95. The different criteria are practical. RF heated plasma can't be purely D or T, because 2-5% of H needs to be present for the H minority scheme to work, and often in T plasmas the breakdown and termination were done with H to save T, so early and late ohmic transitions sometimes have lower c_T. In plasmas labelled as DT the T concentration ranged from 0.47 to 0.71.

We show in Figs 1 a typical example of L-H transition experiment in D and in Fig.2 an L-H transition experiment in DT. They share some characteristics and differ in others.

When Neutral Beam Injection (NBI) is used for plasma heating, main ion temperature measurements (T_i) can be made with the core Charge-Exchange diagnostic [28]. The measurements require on/off modulation of the particular Positive Ion Neutral Injectors (PINI) within the line of sight of the diagnostic (in Octant 8), compensated by on/off modulation of a PINI from Octant 4 (not visible to the CX diagnostic). In the NBI heated L-H experiments shown in Figs. 1 and 2 the bottom 1 MW of auxiliary heating is constructed with the core CX PINI (in blue) turned on/off for 100 ms periods, with the compensating PINI shown in magenta. In L-H transition experiments the active PINIs are operated at low voltage to reduce the power per PINI to ~1 MW. This doesn't affect the quality of the CX measurement and helps smooth the power ramps, at the cost of increased Tritium consumption.

Electron density and temperature profiles can be measured with the High Resolution Thomson Scattering system (HRTS), which provides profiles near the plasma equator every 50 ms. For B_{tor} > 2T density profiles can be profile measured with high time resolution with a profile reflectometer, and Doppler reflectometry analysis can measure the perpendicular rotation of the fluctuations, related to the radial electric field, E_r.

Line averaged densities can also be measured with the interferometer array every 1 ms or faster. Relevant lines of sight of both diagnostics are shown in Fig. 3, together with typical L-mode profiles just before the transition. For the profile in Fig. 3, the value of $\bar{n}_e$ is marked by the height of the black horizontal line extending from the core (vertical blue line at 3.034 m) out to 3.9 m. That is the region of the plasma that contributes to the core line average, $\bar{n}_e$. Correspondingly the value of $\bar{n}_{e,edge}$ is marked by the height of a short black horizontal line, from the dashed vertical blue line at R=3.73 m out to the edge. Although the figure is somewhat complex, the message is that for the flat density profiles typical of L-mode, core line averaged density, $\bar{n}_e$, is in fact very similar to the density at the top of the pedestal, while the edge line averaged density, $\bar{n}_{e,egde}$, actually represents about 2/3 of the pedestal density. If the L-H transition is linked to local density or density gradient values, a critical value of $\bar{n}_e$ may order the data better. On the other hand, as already shown in Figs 1 and 2, $\bar{n}_{e,egde}$ provides a better variable to identify that a transition has taken place. We will display our threshold data as a function of both variables.

In typical L-H transition experiments the heating power is ramped slowly, so the pre-transition state and the critical
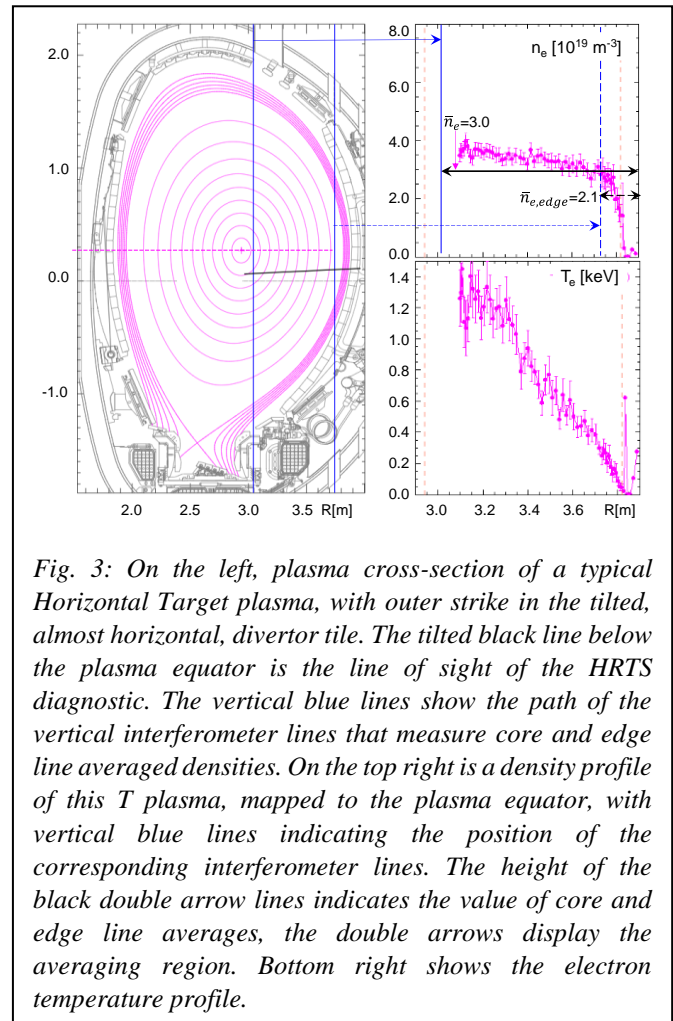

Fig. 3: On the left, plasma cross-section of a typical Horizontal Target plasma, with outer strike in the tilted, almost horizontal, divertor tile. The tilted black line below the plasma equator is the line of sight of the HRTS diagnostic. The vertical blue lines show the path of the vertical interferometer lines that measure core and edge line averaged densities. On the top right is a density profile of this T plasma, mapped to the plasma equator, with vertical blue lines indicating the position of the corresponding interferometer lines. The height of the black double arrow lines indicates the value of core and edge line averages, the double arrows display the averaging region. Bottom right shows the electron temperature profile.

power required to obtain such transition are found experimentally. L-H transitions can be identified, typically by a drop in Balmer α light in the inner divertor region taking place at the same time as an increase on edge density and plasma energy. Sometimes the transitions are very subtle and an analysis of the profiles and the pedestal MHD are required.

To hold the density constant while the power is ramped up we can use active feedback on the gas injected: initially gas injection is increased to compensate the loss of particle confinement due to increasing power in an L-mode. In Fig. 1 we show an example of a Deuterium L-H experiment with active density feedback: oscillations of density (Fig. 1b) and gas (estimates shown in Fig. 1d) are common with this set-up because in JET the GIMs are relatively slow and no time was devoted to optimisation of the feedback system in this case. Here we must point out that measurement of the amount of gas injected by these gas valves is difficult in this case for technical reasons, both estimates shown in Fig 1d come with large uncertainties, but the trends described are correct. Despite those uncertainties, we do observe that soon after the L-H transition the density rises and as a consequence the gas

is turned off by the feedback system. This change in particle source makes it difficult to compare particle transport in the L and H phases.

For typical L-H transition experiments with NBI it is important to avoid sudden jumps or large steps on power delivered to the plasma. Power ramps can be created with the Neutral Beam Local Manager (NBLM) [29]: different PINIs are turned on and off to smooth the power ramp. NBI power modulation works best when multiple PINIs are available on back-up, so a different one can be chosen when a particular PINI fails to deliver the expected power. Careful design of the power ramps is needed to avoid sudden power changes, as observed at 12.3 s in Fig. 1 (luckily after the 1st L-H transition), when there is a transient 2 MW blip of NBI power.

Experiments can also be executed with constant gas input in feed-forward: after an initial transient at power turn-on the density settles or evolves rather slowly, so the power threshold for the transition can be measured at nearly constant gas and density. An example of a Deuterium-Tritium L-H transition experiment executed at constant gas is shown in Fig. 2. Note that in this case the pedestal density rises more sharply at the transition, since the particle source remains constant.

Fig. 2 also illustrates various choices required by operation with Tritium. To minimise consumption of T gas injected per shot an optimise gas injection measurements we opted for feed-forward control of Tritium injection. On NBI heating we opted for 1 MW power steps rather than ramps with modulated power, as shown in Fig. 2a. Fig 2d shows gas injected, with uncertainties during the constant phases of order 10%. Further, when possible we programmed two power ramps per shot, in the hope of obtaining two measurements of P_{LH} at two different densities in 1 shot, as in Fig. 2, without the additional Tritium consumption associated with beginning and end phases of the plasma. These choices reduce expected Tritium consumption by about half. But they are not without consequences: for instance, the plasma state after the 1st power ramp ends is not always adequate to measure P_{LH} with the 2nd ramp. We will discuss one example of this later on.

In the 2021 Tritium campaign it soon became evident that there was a Tritium containment issue related to the NBI system in Octant 4: only Octant 8 was available. There were fewer PINIs available for the NBI power ramps (half at best), and T_i measurements had to be made via infrequent uncompensated notches in the CX PINI.

Other constraints on experiment planning include the cancellation of a Hydrogen campaign with H-NBI heating, originally planned before the 1st T campaign. This might have allowed us a better characterization of L-H transitions, L and H-modes in H plasmas, with better diagnostics.

Whenever possible we carried out L-H experiments with Ion Cyclotron Radio Frequency heating (ICRH or RF), in part to alleviate time constraints for experiments that required NBI and also to save Tritium, and in part to investigate differences between RF and NBI induced transitions. In D and T plasmas minority heating of Hydrogen was used (the H concentration was kept at or below 5%), while in H plasmas majority heating was used. Hardware problems of the RF system affected some of our experiments (see discussion about antenna phasing in [10]). Here we present only results obtained with correct RF antenna phasing control.

A review of the JET P_{LH} Carbon wall results [3][30] found that for B_{tor}=1.8 T, I_p=1.8 MA, the 1997 JET isotope dataset encompassed a rather narrow (low) density range, likely to be below $\bar{n}_{e,min}$. With this in mind we designed our isotope experiments in the JET-ILW to measure P_{LH} in a broad range of densities. JET-ILW isotope datasets are collected for 3 different choices of (B_{tor}, I_p), all with the same shape, matching existing datasets in D and H.

3. L-H power threshold measurements

In what follows we show the results of our L-H transition studies for the 3 datasets we have available with well documented isotope transition data. Comparison to scalings will be described in Section 4, selecting high density branch points of the 3 datasets. It is important to obtain datasets with different toroidal fields, since eventually we need to extrapolate to devices with higher field.

All T and DT L-H experiments were carried out with the same plasma configuration, Horizontal Target. That configuration has lower P_{LH} and lower gas consumption, since the outer strike line is far from the divertor cryogemic pump. Within each dataset, B_{tor} and I_p can have variations of order 5%

We should remind the reader that in JET-ILW it was found that the value of $\bar{n}_{e,min}$ for each species appears to be correlated with the ratio of the plasma line averaged density $\bar{n}_e$ to the Greenwald limit density [31] given by n_{GW}= I_p[MA]/π/a^2, with a the plasma equatorial minor radius. We call this ratio f_{GW}= $\bar{n}_e$/n_{GW}, the Greenwald fraction, and display it in the subsequent power threshold plots, with $\bar{n}_e$ along the bottom horizontal axis and f_{GW} along the top horizontal axis.

We report the densities at the time of the transition, and P_{loss} and P_{sep} are averaged over 70 ms before the transition. Typical error bars on P_{loss}, P_{sep}, P_{rad} are of order 10%, not shown in the plots but recognisable in the scatter when enough datapoints are available. Error bars on density are less than 5%.

A further word on data selection: we chose to display datapoints with good RF heating. Early in H and T campaigns there was a problem with the phase control in the RF system and those transitions were found to be unusual, with many dithers and increase in P_{rad} after most transitions, we find it
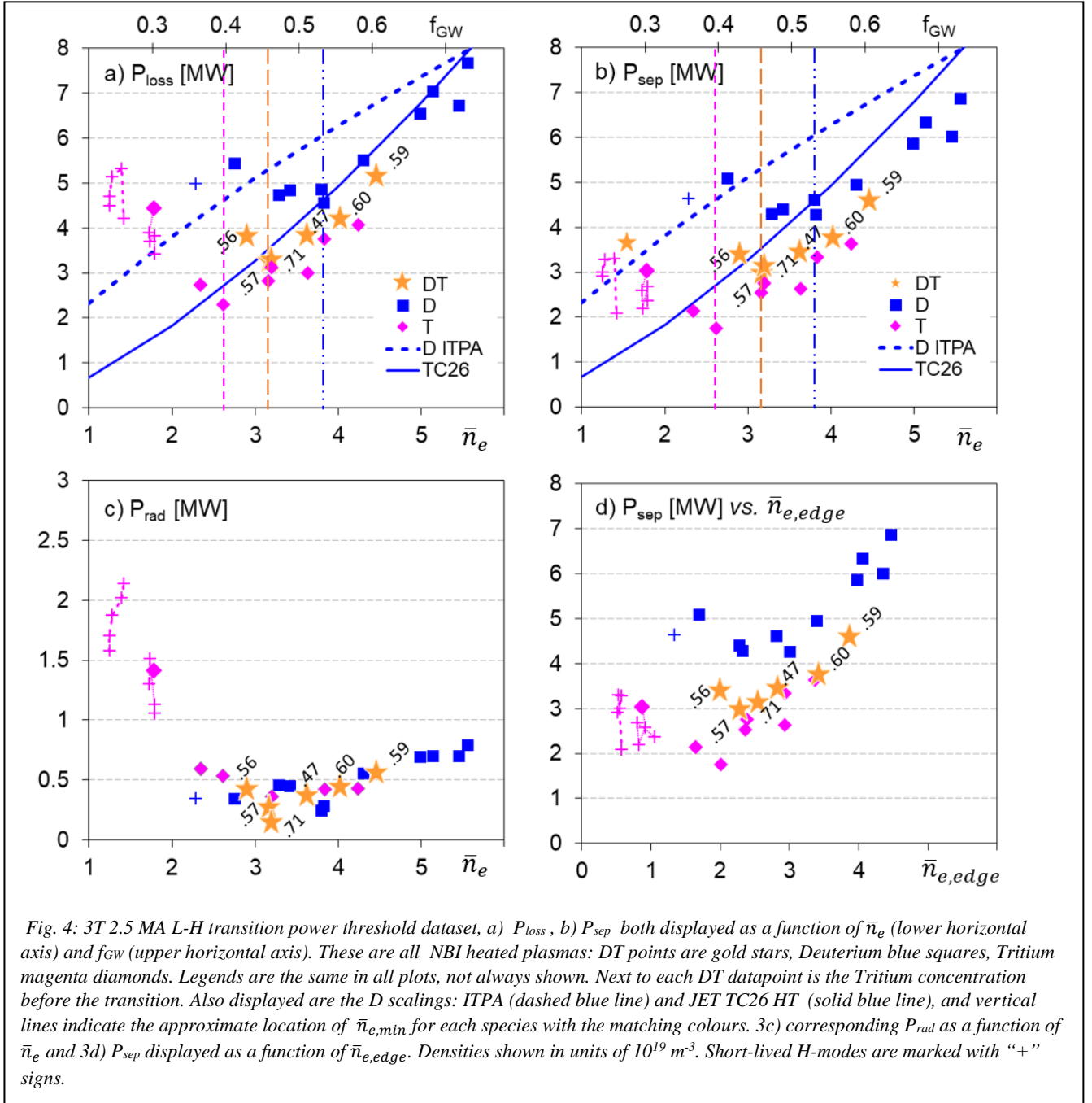
Fig. 4: 3T 2.5 MA L-H transition power threshold dataset, a) P_{loss} , b) P_{sep} both displayed as a function of $\bar{n}_e$ (lower horizontal axis) and f_{GW} (upper horizontal axis). These are all NBI heated plasmas: DT points are gold stars, Deuterium blue squares, Tritium magenta diamonds. Legends are the same in all plots, not always shown. Next to each DT datapoint is the Tritium concentration before the transition. Also displayed are the D scalings: ITPA (dashed blue line) and JET TC26 HT (solid blue line), and vertical lines indicate the approximate location of $\bar{n}_{e,min}$ for each species with the matching colours. 3c) corresponding P_{rad} as a function of $\bar{n}_e$ and 3d) P_{sep} displayed as a function of $\bar{n}_{e,edge}$. Densities shown in units of 10^{19} m^{-3}. Short-lived H-modes are marked with "+" signs.

safest to discard them for this study. Those transitions are described in detail in [10]. Also, transitions in mixed H+T plasmas are described in a separate publication [11].

3. 1. The 3 T 2.5 MA NBI heated P_{LH} dataset.

This is the dataset that allows us to identify $\bar{n}_{e,min}$ for D, T and DT plasmas.

In Fig. 4a and 4b we show the threshold data in the conventional way, as a function of the plasma line averaged density, $\bar{n}_e$. We display f_{GW}, the Greenwald fraction, in the upper axis, since in earlier studies it was found to correlate

with the value of $\bar{n}_{e,min}$ for different plasma species. In Figs. 4c and 4d we show $P_{rad,bulk}$ as a function of $\bar{n}_e$, and P_{sep} as a function of edge line averaged density, $\bar{n}_{e,edge}$. If the relative position of the P_{sep} points changes from 3b to 3d it may indicate unusual plasmas, as we will discuss later on in Fig. 7. All L-H transitions shown are marked with solid symbols, while short-lived or marginal H-modes are displayed with "+" signs, the connection lines between the "+" signs imply there are various such transitions in the same shot. This typically happens in the low density branch, when each sawtooth arrival (or some of them) can drive a short-lived transition into M-mode [32] The M-mode exhibits easily recogniseable

magnetic characteristics, an n=0 m=1 low frequency oscillation, and it is often used to identify L-H transitions.

The Deuterium L-H threshold data, blue squares in Figs. 4, is a mixture of earlier L-H experiments, often with feedback controlled density and modulated NBI, and more recent data, with gas feedforward and NBI power steps. The two types of experiments give comparable results in D. The TC26 scaling, marked with a solid blue line in Figs 4a and 4b, is quite close to the Deuterium P_{loss} datapoints. This is not surprising since that scaling was based on the JET-ILW high density branch D data available at the time for that plasma shape. The ITPA scaling is displayed with a dashed blue line. We have attempted to obtain D L-H transitions at higher f_{GW}, since datapoints near f_{GW}=0.7-0.8 are of most relevance for JET scenarios and for ITER, but we run out of experimental time in D: high density transitions are more complex to perform, they require large amounts of gas throughput and there is a small margin between the L-H threshold and a density limit instability. An additional complication is that the increased neutral pressure produced by the increased gas injection that aims to raise the density results in more efficient pumping, thereby requiring greater injection. For high density L-mode plasms, the gas required to achieve a given target density value increases quadratically with target density.

The T and DT data was obtained with gas feed-forward and NBI steps. T is displayed with magenta diamonds, DT with gold stars. It is clear that as we move from D to DT to T plasmas the value of density at which P_{LH} is minimum, $\bar{n}_{e,min}$, drops, as well as the corresponding $P_{LH,min}$. Next to each DT datapoint we display the Tritium ratio, $n_T/(n_H+n_D+n_T)$, at the time of the L-H transition. Near $\bar{n}_{e,min}(DT)$ both P_{loss} and P_{sep} are very similar for 57% and 71% levels of Tritium concentration.

Both P_{loss} and P_{sep} data display an ordering of the P_{LH} data, with Tritium obtaining the L-H transition at the lowest powers, a little higher in DT, and higher in D. The differences are not very large, especially between DT and T at higher densities.

	f_{GW}	$\bar{n}_e$	$\bar{n}_{e,edge}$	P_{loss}	P_{sep}	P_{aux}
D	0.44	3.8	3.0	4.6	4.3	4.0
DT	0.37	3.2	2.3	3.3	3.0	2.0
T	0.30	2.6	2.0	2.3	1.75	1.0

Table 1. Values of $\bar{n}_{e,min}$ for the 3T 2.5 MA Horizontal target dataset.

The change in $\bar{n}_{e,min}$ has interesting consequences: in T at $\bar{n}_{e,min}(T)$ a transition is observed with only 1 MW of NBI, while in DT, at $\bar{n}_{e,min}(DT)$, 2 MW of NBI are required, and in D at $\bar{n}_{e,min}(D)$ 4 MW of NBI are required. This suggests it might be useful to consider a Tritium rich plasma at the start of the H-mode transition for DT pulses in ITER or DEMO to facilitate H-mode access, if it is found that the power required to access H-mode is larger than expected. Further, a T-rich plasma would have better absorption of RF heating, as

discussed in [40].

At the moment the strategy to enter H-mode in ITER in DT is to start the pulse in D, to save T, then increase Tritium level to that similar of D and apply higher D-NBI and RF heating. In the present plan this could be in the current flat top or during the current and density ramp, to take advantage of the reduced threshold and $n_{e,min}$ at lower plasma current and the more gradual increase of alpha heating in those conditions. In the alternate scenario we propose, entry into H-mode at low density and low P_{LH} in a T-rich plasma would lead to a rise in density due to the H-mode, without additional T injection. This lower P_{LH} with higher T concentration, and increased RF absorption, needs to be balanced with possible increased radiation in a T-rich plasma, the lack of alpha heating after H-mode transition until the D density is raised and the possibility of increased T-throughput per pulse when such approach is followed. Detailed simulations will be necessary to ascertain which route is most promising, and to which scenarioit may apply best. Indeed such an approach was considered in the ITER Research Plan [24] (see section 2.6.5.3) as an option for better control of H-mode access in the long pulse and steady-state scenarios should 50-50 DT plasmas present complex control issues in this phase.

The accessible window for H-mode in SPARC has been shown to be sensitive to the L-H threshold power (cf. fig 2 in [41]) and a lower threshold associated to a T-rich plasma would open a wider DT operational window at full field and current. This may be true for other fusion devices as well.

For DT plasmas we have fitted the experimental profiles, using them as input to TRANSP interpretive simulations. We found good agreement between database evaluations of absorbed power and TRANSP results. We established that for DT plasmas P_{fus} is at most 50 kW, smaller than the expected errors in the measurements, making no significant contributiom to P_{LH} evaluation.

In Tritium at the lowest densities large bulk radiation contributes to large P_{loss}, but P_{sep} also clearly shows that these plasmas are in the low n_e branch. Large bulk radiation is likely due to enhanced W sputtering in Tritium bringing impurities (often Be, sometimes W) into the plasma and cooling it. Below $\bar{n}_e$=2×10^{19} m^{-3} the L-H transitions took the plasma into M-mode, and often into brief H-mode states, denoted with "+" signs. ELM-free phases followed by clear ELMs only took place above $\bar{n}_e$=3.3×10^{19} m^{-3}. At that density the Tritium plasmas are already in the high density branch.

In these NBI heated plasmas, as long as density is not too low, radiation is small, typically of order 0.5 MW, as shown in Fig. 4c.

For this dataset, in D, we tested injection of CD_4 as a possible means of increasing signal and acquire edge Charge-Exchange T_i and V_{tor} measurements (the natural level of C impurities in the plasma dropped below detection after C was replaced by Be walls and W divertor). We found that an amount of CD_4 that was still insufficient to provide good quality edge CX measurements increased P_{sep} at the same
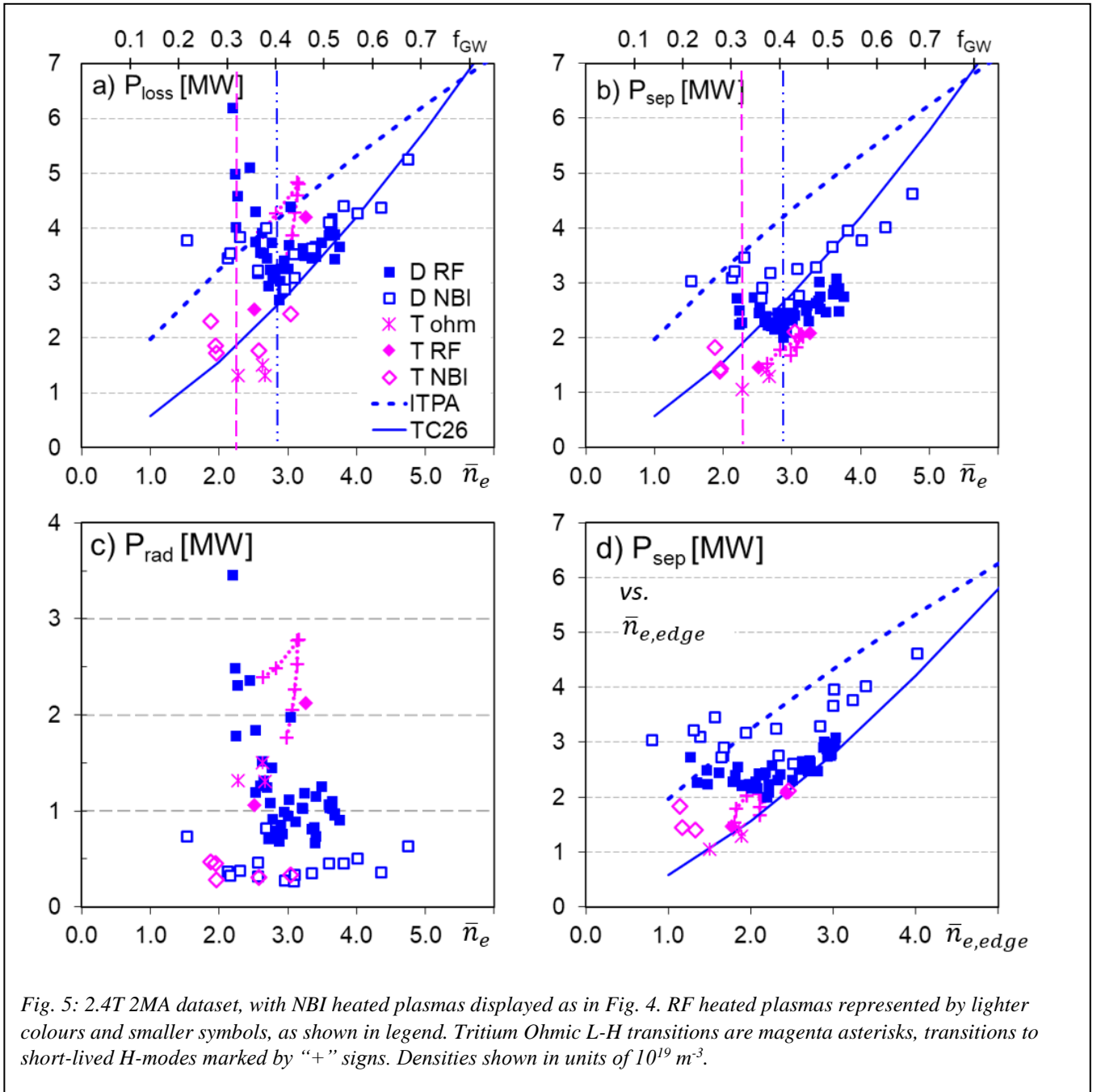
Fig. 5: 2.4T 2MA dataset, with NBI heated plasmas displayed as in Fig. 4. RF heated plasmas represented by lighter colours and smaller symbols, as shown in legend. Tritium Ohmic L-H transitions are magenta asterisks, transitions to short-lived H-modes marked by "+" signs. Densities shown in units of 10^{19} m^{-3}.

density by at least 1 MW. We decided to do L-H experiments without CD_4 injection and therefore without edge CX measurements, rather than struggle to deconvolve Carbon effects from other dependencies of P_{LH}.

At this toroidal field it is possible to measure the radial electric field, E_r, with Doppler reflectometry. The analysis of E_r profiles before the transition, and hopefully of E_r evolution along the power ramp for these plasmas will be the subject of a future publication. We have began the study of the possible relationship between $\bar{n}_{e,min}$ and the ion heat flux for this dataset, continuing earlier work in D in JET-ILW [39].

3.2. The 2.4 T 2 MA P_{LH} dataset

This is our most studied dataset in D, since experiments can be executed at relatively low power, allowing the study of L-H transitions with either Rf or NBI heating, while at the same time the magnetic field is high enough to enable reflectometry measurements of density profiles and Doppler reflectometry.

At this field and current P_{LH} can be low enough that ohmic L-H transitions were observed in Tritium, and it is also possible to obtain L-H transitions with RF heating alone. The plots shown in Fig. 5 display NBI and RF transitions in D and T, as well as an Ohmic transition in T near $\bar{n}_{e,min}$.

For RF heated plasmas the RF frequency was 42 MHz, which locates the H resonance at R=2.6 m, near the normalised poloidal flux surface Ψ_N= 0.16, inboard of the sawtooth inversion radius in the high field side. This avoids large sawteeth, which could bring a dominant term to P_{LH} at low density.

The P_{loss} plot in Fig. 5a shows similar power thresholds for NBI and RF in D. As shown in 4c, radiation is much higher for RF heated plasmas both in D and T. This is likely due to higher sputtering produced by RF sheath effects, and/or by RF

	f_{GW}	$\bar{n}_e$	$\bar{n}_{e,edge}$	P_{loss}	P_{sep}	P_{aux}
D	0.45	2.9	2.2	2.7	2.0	1.8
T	0.33	2.3	1.5	2.4	1.3	0

Table 2. Values of $\bar{n}_{e,min}$ for the 2T 2.4 MA Horizontal target dataset.

heated fast H ions. Once radiation is discounted, P_{sep} for D is lower for RF heated plasmas than for NBI heated plasmas, but the difference is negligible in T plasmas. In T plasmas in the high density branch some H-modes are not steady (displayed with "+" signs): as the density rises with the H-mode, the radiation increases and the plasma drops out of H-mode. When P_{rad} is removed (P_{sep} in Fig. 5b), the data points fall in line with the conventional transitions.

Table 2 shows $\bar{n}_{e,min}$ values, but there is vertical scatter in the data. We will later on choose a higher density as the bottom of the high density branch, to ensure we only label as high density branch datapoints that show an increasing trend of P_{sep} vs. $\bar{n}_e$.

Again the TC26 scaling matches the D data better than ITPA 2008. We failed to obtain higher $\bar{n}_e$ points, which might have improved the identification of the $\bar{n}_e$ scaling coefficient.

In Deuterium plasmas at this field and current E_r measurements have shown comparable profiles at the transition at similar n_e, regardless of heating method, NBI or RF [33] More strikingly, in D the E_r profile doesn't appear to evolve along the power ramp, despite the fact that the electron pressure gradient does increase (in magnitude) with power. For this field and current we have also analysed the effect of plasma configuration on the L-H transition [34]. It was found that the edge perpendicular flow was significantly affected by changes in the divertor configuration in the region inside the separatrix, without providing an explanation for the very different power thresholds.

We recall that for this dataset it has been shown [6] that $\bar{n}_{e,min}$ and P_{LH} decrease with plasma current, I_p: with I_p=2 MA, $\bar{n}_{e,min}$=2.9×10^{19} m^{-3} and P_{RF}=1.8 MW, while with I_p= 1.5 MA, $\bar{n}_{e,min}$=2.2×10^{19} m^{-3} (or less) with P_{RF}=1.1 MW. In both cases f_{GW}=0.42. That D data supports the ITER strategy of entering H-mode at low current and density. We have no data on the possible I_p dependency of P_{LH} in T or DT.

	f_{GW}	$\bar{n}_e$	$\bar{n}_{e,edge}$	P_{loss}	P_{sep}	P_{aux}
H	0.54	3.1	2.3	5.3	4.0	7.7
D	0.38	2.2	1.6	1.7	1.5	1.0
T	0.40	1.4	0.8	1.1	0.9	0

Table 3. Values of $\bar{n}_{e,min}$ for P_{sep} in the 1.8 1.7 MA

3.3. The 1.8 T 1.7 MA P_{LH} dataset

This dataset allows us to compare P_{LH} for H, D and T plasmas, the largest isotope range. It has already been presented in part in [7], [10], [11]. We have obtained a few additional datapoints in D and DT, which help us complete the description of our results. We do not address here the scans in Tritium concentration in plasmas with varying concentrations of H and T, described in detail in [10] and [11].

Results are displayed in Fig. 6, as for the previously presented datasets. We see that in H P_{loss} is minimum at 2.92 10^{19} m^{-3}, while P_{sep} has a minimum at 3.14 10^{19} m^{-3}.

As before, we see that TC26 reflects accurately the P_{loss} threshold of the high density D branch. Since for D plasmas in the high density branch P_{rad} is small, P_{sep} is also close to the TC-26 scaling, below the ITPA one. In terms of P_{loss} we see little difference between threshold values for D, DT and T plasmas in Fig. 6a, and both are much lower than the H values. When radiation is subtracted in Fig. 6b we observe that P_{sep}(T) < P_{sep}(D) in general, and both < P_{sep}(H), with the possible exception of the high density NBI heated datapoint marked with a black circle (discussed later), especially when viewed as a function of edge density, in Fig. 6d. It does appear that RF heated plasmas in T have lower P_{sep} than the NBI heated ones.

The most striking feature of this dataset is that NBI heated Hydrogen plasmas exhibit much higher P_{LH} than RF-heated ones [8], [5]. Until recently we have considered two possible explanations for it, based on the impact of the heating method on the E_r profile. On the one hand, if NBI induces co-rotation in the plasma, and if the radial electric field is dominantly given by the v×B term, then co-I_p NBI might reduce the E_r well depth, as reported in [35]. On the other hand, if E_r is dominated by the ion pressure gradient, RF H majority heating may deepen the E_r gradient more effectively than NBI heating [10]. Alas, we lack edge CX rotation measurements, and for this dataset we also lack E_r measurements (the field is too low). But maybe impurities provide another explanation: we have recently learned that the H-NBI heated H plasmas had significant Cu content, which may have affected L-mode confinement and therefore the power threshold [36]. This could explain the fact the NBI heated plasmas had larger radiation in H than in D and T, although it doesn't explain why P_{sep} is also higher for these NBI heated H plasmas.

The RF heating scheme for H plasmas was H-majority heating, 2nd harmonic resonance at 51 MHz, at R= 3.19 m,

outboard of the magnetic axis. Instead, in D and T plasmas we used Hydrogen minority heating (typically $n_H/n_e < 5\%$), 1st harmonic resonance at 33 MHz, resonant at 2.46 m. Typically in these pulses the inversion radius was at 2.63 m inboard and 3.25 m outboard. Off-axis deposition was chosen to ensure small, frequent sawteeth, which is a beneficial situation for L-H transition studies, since often sawtooth arrival at the edge can trigger transitions.

In RF-heated H plasmas radiation is dominated by medium Z impurities (Ni, Cu), brought in by the interaction between plasma and antennae. In general RF sheath rectification effects especially at the lowest densities and for the heavier isotopes. This might explain why radiation is high for RF heated T

plasmas at medium densities, and for D at low densities.are known to accelerate all ions in the SOL, even more so in D and T plasmas, possibly increasing Be and W sputtering,

In Tritium we observe ohmic transitions for densities below 2.5×10^{19} m^{-3}, $f_{GW} = 0.4$. Ohmic heating can't be controlled externally without changing the plasma current, and P_{loss} is quite flat as a function of density from 0.25 to 0.4 n_{GW}. We have no information on a low density branch in this case. At higher densities we observe large radiation in RF-heated T plasmas, about half of it attributable to W.
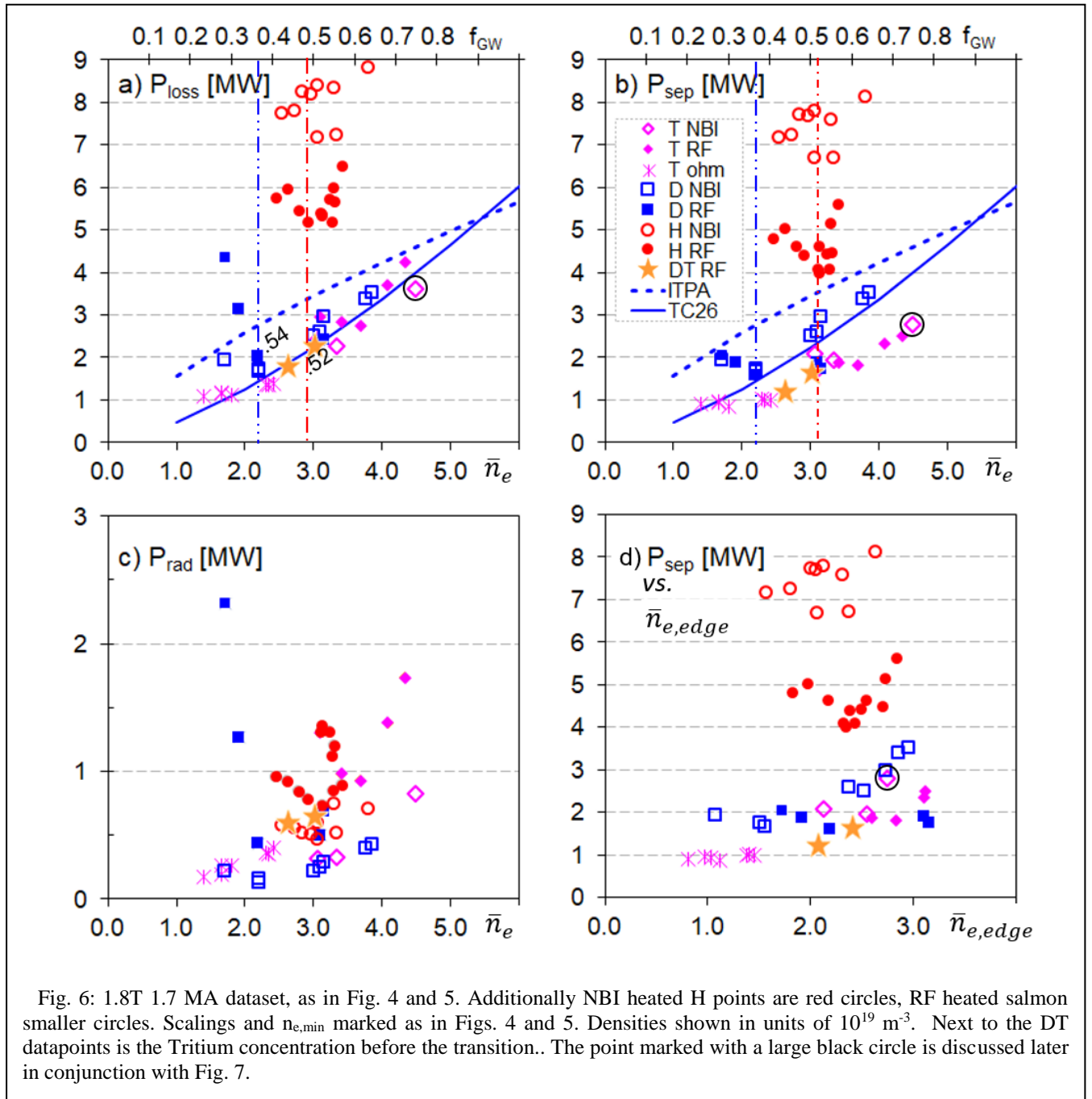
Fig. 6: 1.8T 1.7 MA dataset, as in Fig. 4 and 5. Additionally NBI heated H points are red circles, RF heated salmon smaller circles. Scalings and $n_{e,min}$ marked as in Figs. 4 and 5. Densities shown in units of 10^{19} m^{-3}. Next to the DT datapoints is the Tritium concentration before the transition.. The point marked with a large black circle is discussed later in conjunction with Fig. 7.
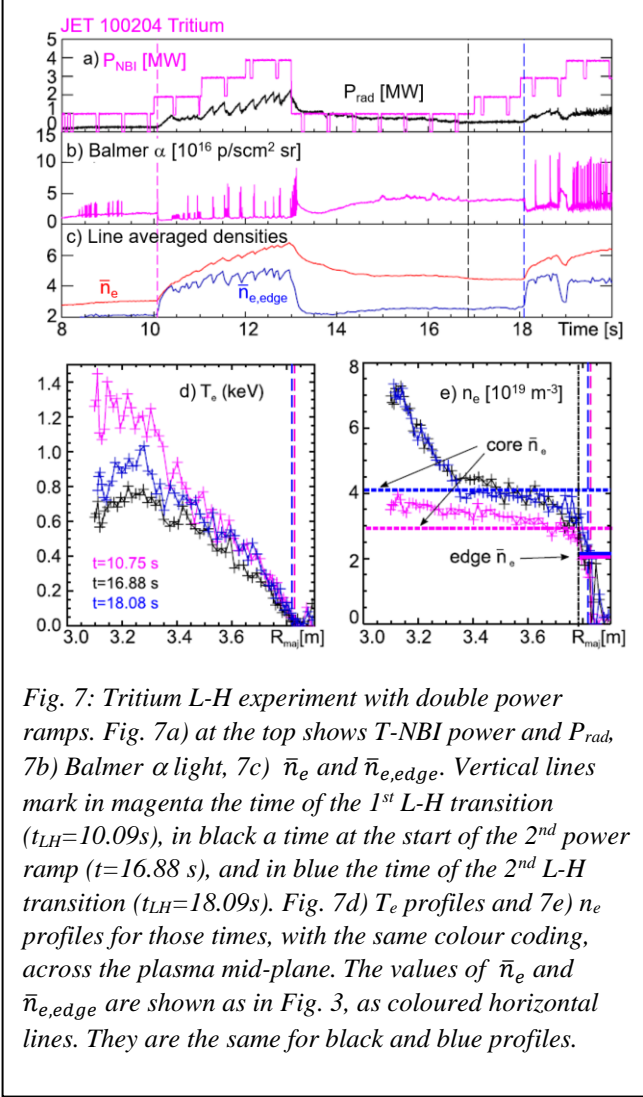
Fig. 7: Tritium L-H experiment with double power ramps. Fig. 7a) at the top shows T-NBI power and P_{rad}, — *Fig. 7a) at the top shows T-NBI power and P_{rad}, 7b) Balmer α light, 7c) $\bar{n}_e$ and $\bar{n}_{e,edge}$. Vertical lines mark in magenta the time of the 1st L-H transition ($t_{LH}=10.09s$), in black a time at the start of the 2nd power ramp (t=16.88 s), and in blue the time of the 2nd L-H transition ($t_{LH}=18.09s$). Fig. 7d) T_e profiles and 7e) n_e profiles for those times, with the same colour coding, across the plasma mid-plane. The values of $\bar{n}_e$ and $\bar{n}_{e,edge}$ are shown as in Fig. 3, as coloured horizontal lines. They are the same for black and blue profiles.*

The highest density NBI heated T transition (marked as a large magenta diamond surounded by a circle in Figs. 6) took place on the second power ramp of the plasma pulse, and W had already penetrated in the plasma core after the earlier H-mode phase. That transition is illustrated in Fig. 7 (blue vertical dashed line at 18.08s), showing that its preceding L-mode had profiles typical of W-poisoned plasmas, with peaked n_e profiles and somewhat hollow T_e, quite different from the pre-transition profiles from the transition in the 1st power ramp, at 10.075s (same as in Fig. 3). The study of this particular outlier lead us to investigate the relationship between the core and edge line averaged densities, $\bar{n}_e$ and $\bar{n}_{e,edge}$ respectively with the pedestal density, $\bar{n}_{e,ped}$. A comparison of line averaged densities with the corresponding density profile in Fig. 7e) shows that for the L-H transition in the first power ramp, marked in magenta, $\bar{n}_e$ is a good proxy for the pedestal density, while $\bar{n}_{e,edge}$ is too low to represent the pedestal height, as discussed earlier. When the profiles are atypical, as in the black and blue times and profiles that have

strongly peaked density profiles due to W contamination, we observe that the relationship between $\bar{n}_e$ and pedestal density changes: $\bar{n}_e$ is now considerably higher than the pedestal density, due to the excessive contribution from the plasma core. In all cases $\bar{n}_{e,edge}$ remains too low to caracterise the pedestal density, but it provides a more local measurement, unaffected by the W poisoning.

4. Comparison to scalings

For each dataset we have identified the density beyond which P_{sep} clearly increases as density increases: the bottom of the high density branch, called $\bar{n}_{e,bottom}$. It can be higher than $\bar{n}_{e,min}$ for three reasons: sometimes the P_{LH} minimum is quite flat, or there is vertical scatter in the measurements, and in some cases the minimum hasn't been identified (for instance, the ohmic transitions in Tritium). The values for each dataset and species are displayed in Table 4. A linear fit of the bottom density values of D datasets to B_{tor} results in the function f(B_{tor})=1.35 B_{tor}-0.277 with R^2=0.99, and P_{sep} at the minimum $P_{sep,min}$= 2.307 B_{tor} -2.936 with R^2= 0.88. If instead we base the fits on plasma current, I_p, we obtain f(I_p)=2.012 I_p -1.195 with R^2=0.998, and $P_{sep,min}$=3.571 I_p-4.779, with R^2=0.956. This is consistent with the evidence of lower P_{LH} at lower I_p at low densities. We lack dedicated L-H experiments to explore the dependence of $\bar{n}_{e,min}$ on I_p for fixed B_{tor}.

Having established which datapoints belong to the high density branch we display them together as a function of density in Fig. 8. To simplify the figure we don't distinguish RF and NBI heating as we did in Figs. 4-6.

In Fig 9a and 9b we compare P_{loss} and P_{sep} with the isotope adjusted ITPA scaling.

$$P_{ITPA,iso} = 0.049 \, n_{e20}{}^{0.72} \, B_T{}^{0.8} S^{0.94} (2/A_{eff})$$

as described in [10]. We see in Fig 9a and 9b that both P_{loss} and P_{sep} are considerably lower than the ITPA scaling, for all species. But as discussed earlier, due to the large radiation of T plasmas, we find it more productive to consider P_{sep}, which

	B_{tor}	I_p	f_{GW}	$\bar{n}_e$	$\bar{n}_{e,edge}$	P_{loss}	P_{sep}
D	3.0	2.5	0.44	3.8	3.0	4.6	4.3
DT	3.0	2.5	0.37	3.2	2.3	3.3	3.0
T	3.0	2.5	0.30	2.6	2.0	2.3	1.75
D	2.4	2.0	0.45	3.1	2.6	3.5	2.7
T	2.4	2.0	0.33	2.3	1.5	1.3	1.1
H	1.8	1.7	0.54	3.1	2.3	5.3	4.0
D	1.8	1.7	0.38	2.2	1.6	1.7	1.5
T	1.8	1.7	0.40	2.3	1.4	1.4	1.0

Table 4. Values of density at the bottom of the high density branch, in Horizontal Target plasmas with corresponding f_{GW}, P_{loss} and P_{sep} in H, D, T and DT L-H transitions in JET-ILW

is near 60% of the ITPA expectation. As discussed in [10], this is in part due to the reduced P_{LH} in metal wall devices [4], [23], and in part due to the fact that we are subtracting radiation, while the ITPA scaling was originally derived for P_{loss}, with plasmas that had low radiation. Aside from a possible correction factor to take into account these known dependencies, we find that the datapoints with the highest leverage on the density scaling are the ones with highest threshold: D in 3T 2.5 MA at the highest densities and NBI-heated H at 1.8T 1.7 MA. This suggests that future experiments in H and D might complement our data very usefully.

The comparison of our data and the isotope-adjusted TC26 scaling is displayed in Fig 10a, 10b. As is to be expected, TC26 fits the Deuterium P_{loss} data quite well (it was based on the P_{loss}(D) data available at the time), but both T and NBI-heated H data escape above its predictions. If we compare P_{sep}

to TC26 we see that only NBI-heated H and a couple of T points are above the dashed line that is 20% higher than the scaling, and only the 2.4 T RF-heated D data escapes below 80%.

To better display our data range, we show P_{sep} vs TC26 in a log-log plot in Fig. 11 from 1 to 10 MW. Here we better appreciate that the lowest threshold DT point, at the lowest density at 1.8 T 1.7 MA, is 20% below the TC26 expectation, and there is quite some scatter in the RF-heated T data. On the other hand, the 3T 2.5 MA DT points line up quite well with it, except the one at $\bar{n}_{e,min}$ which is nearly 20% above.

In general, although it is clear that T has lower threshold than D, lower than H, it remains unclear if the assumption that the isotope dependence of P_{LH} is proportional to $(2/A_{eff})$ is quantitatively correct. We would have to analyse the data presented in this article in conjunction with the study of the power threshold in Hydrogen+Tritium mixtures before
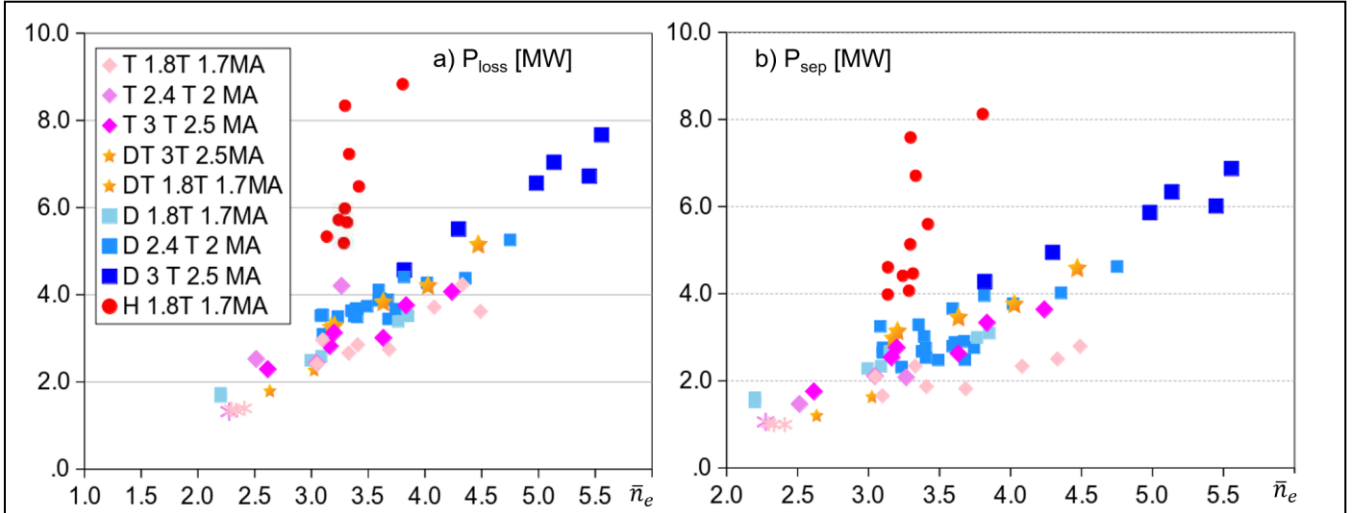

Fig.8: a) P_{loss} and b) P_{sep} as a function of $\bar{n}_e$ for all datasets. Darker shades and/or larger symbols correspond to higher B_{tor}, I_p. Red circles are H, Blue squares are D, Magenta-pink are T, and orange stars are DT.
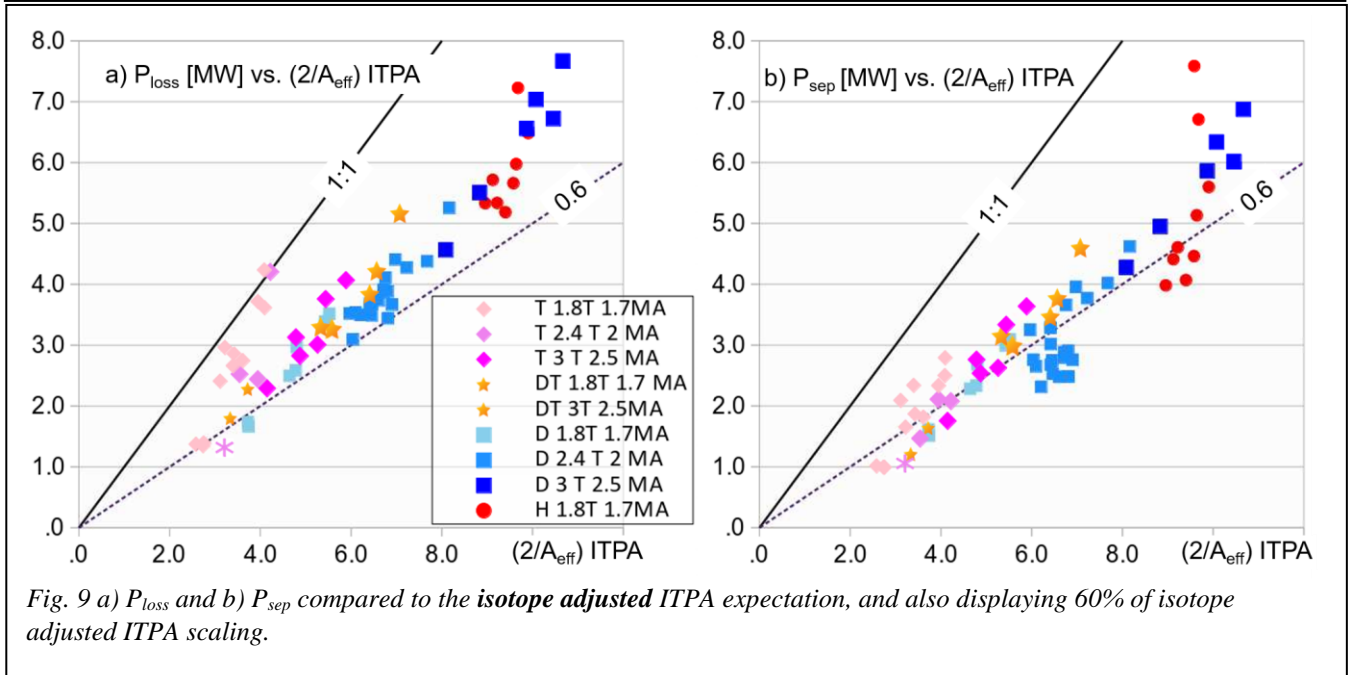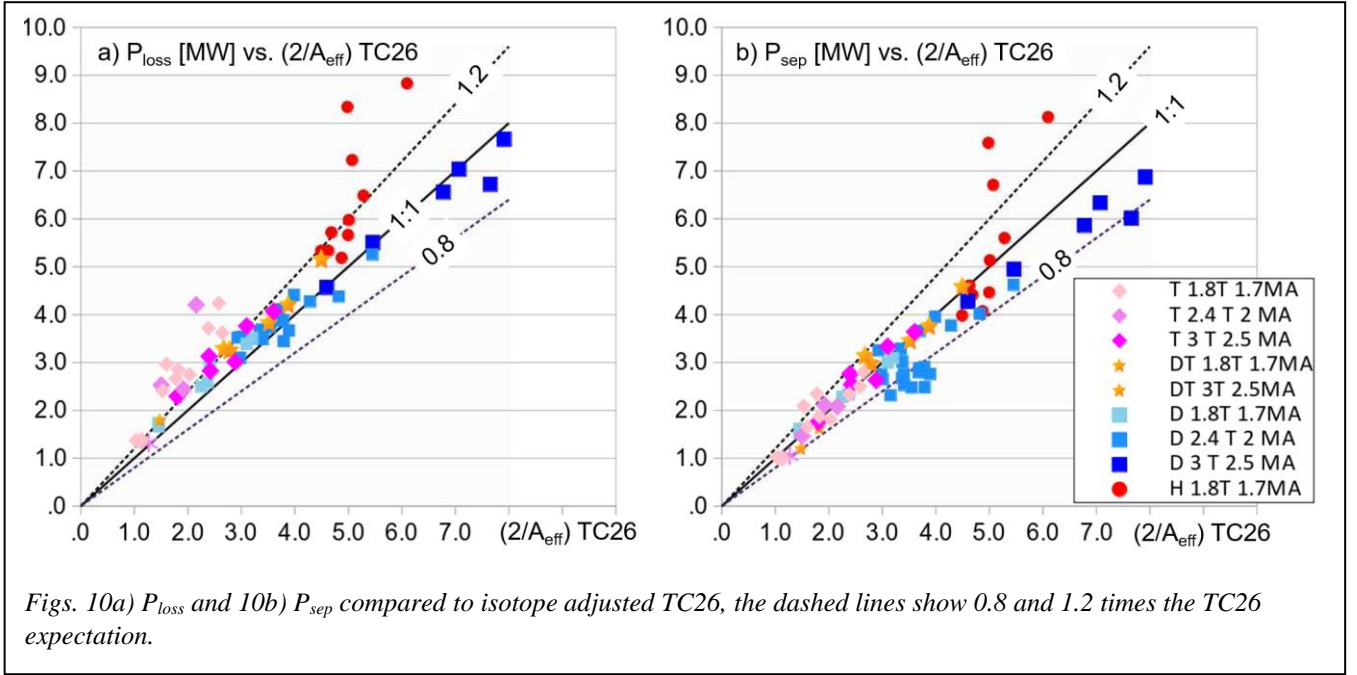

*Fig. 9 a) P_{loss} and b) P_{sep} compared to the **isotope adjusted** ITPA expectation, and also displaying 60% of isotope adjusted ITPA scaling.*

Figs. 10a) P$_{loss}$ and 10b) P$_{sep}$ compared to isotope adjusted TC26, the dashed lines show 0.8 and 1.2 times the TC26 expectation.

arriving at clear conclusions on P$_{LH}$ isotope scaling.

5. Discussion, conclusions and future work

The plots shown in Sections 3 and 4 clearly illustrate that the isotope adjusted ITPA scaling overpredicts P$_{loss}$ and P$_{sep}$ required for the L-H transition in the JET-ILW. But here we must recall that in JET both P$_{loss}$ and P$_{sep}$ can be at least a factor of 2 higher in Corner or Vertical Target configuration, so we cannot use the predictions from Horizontal Target plasmas on their own to modify the ITER guidelines for L-H power threshold evaluations until that effect is understood. The same can be said of the lower than predicted P$_{sep}$ thresholds in RF-heated D plasmas, still not understood.

Deriving a new scaling from all the JET-ILW isotope data is far from trivial, and is beyond the scope of this manuscript, as we need to investigate configuration effects further before extrapolating from Horizontal to Vertical Target plasmas.

It is very clear from our data that $\bar{n}_{e,min}$ and the corresponding P$_{sep,min}$ observed in the Horizontal Target configuration depend strongly on A$_{eff}$, being highest for H, medium for D and lowest for T, for any given dataset, with the possible exception of the ohmic transitions in T at 1.8 T. This is in stark contrast with AUG studies, in mixed currents and fields, which show no difference in $\bar{n}_{e,min}$ between H and D [37], [38]. The AUG results have driven the assumption that in ITER $\bar{n}_{e,min}$ is species independent, and near f$_{GW}$=0.4. That value is in fact not so far off from our observations in D, reported in Table 3, but we do observe, against AUG and ITER assumption, that T has lower $\bar{n}_{e,min}$ and P$_{LH,min}$ than D in plasmas with auxiliary heating.

The strong scaling of P$_{Aux,min}$ with A$_{eff}$ does suggest it may be easier to enter H-mode in T-rich plasmas in any future DT fusion devices and experiments. This may be aided by the observed increased absorption of RF power in T-rich plasmas [40], if RF is applied during the L-H transition phase.

Studies of P$_{LH}$ in H-T, DT mixtures compared to H and D plasmas are being published elsewhere [10], [11] and have not been reviewed here, but will need to be taken into consideration to make scalings and predictions. They were carried out only at 1.8T 1.7 MA in Horizontal Target plasmas. They show that P$_{LH}$ does not simply scale with A$_{eff}$, not even in the high density branch of a single dataset: at the same $\bar{n}_e$ P$_{LH}$(D) isn't the same as P$_{LH}$ for a 50/50 mixture of H and T.

The results presented here are the starting point for a variety of more detailed studies, especially in terms of investigating critical profiles (kinetic and E$_r$) before the transition, and models for $\bar{n}_{e,min}$ variation. Similarly to the work done for D-only plasmas [39], work is underway to carry out a power balance analysis, characterise the role of ion and electron channels at the transition, and investigate if the ion heat flux can explain the changing values of $\bar{n}_{e,min}$ in D, DT and T plasmas.

Work is underway to use profile evolution information from these experiments to validate transport models and L-H transition models, and hopefully contribute to make physics-based predictions of L-H threshold conditions. In particular the analysis of E$_r$ profiles before the transition, and hopefully of E$_r$ evolution along the power ramp for DT and T plasmas will be the subject of a future publication.

In time, we aim to analyse the threshold data as a function of true pedestal density, probably more closely aligned to the physical mechanisms of the L-H transition. We propose to undertake a systematic study of the possible dependence of P$_{LH}$ on $\bar{n}_e$ vs. $\bar{n}_{e,edge}$ or $\bar{n}_{e,ped}$, or even their gradients. It may help us understand the relative importance of local and global conditions on the transition itself.

Fig. 11: Same as 10b, but in log-log plot.
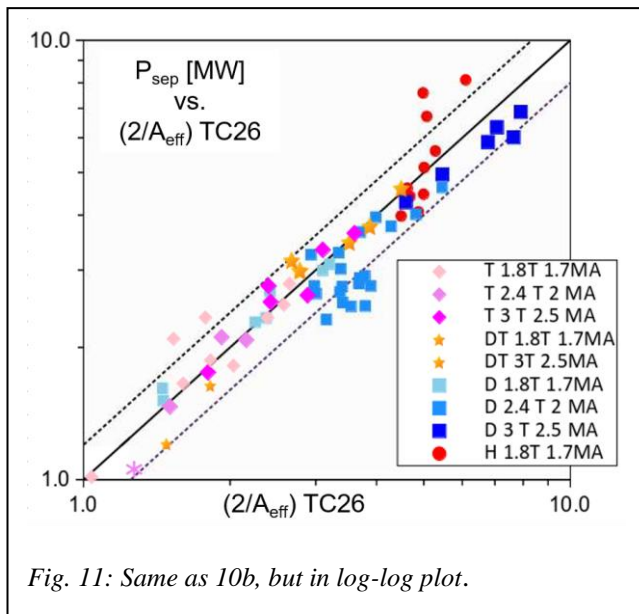
In forthcoming JET campaigns we hope to obtain a few additional data points to better characterise low and high density transitions. In D we will request data at 1.8T near the minimum, and both in D and T we would benefit from obtaining data above $f_{GW}=0.7$, which is the lower bound of the typical H-mode operational space, and would provide information that most clarifies the density scaling of P_{LH}. We also hope to obtain additional L-H experiments in D in the Corner configuration, typical of the record DT shots. Ideally an H campaign with H-NBI heating might allow us to understand the very high P_{LH} of H plasmas, or correct our earlier observations, if the high threshold was due to excessive Cu content and its consequences.

The effort of carrying out systematic L-H transition experiments in H, D, DT and T in the JET-ILW provided a wealth of data and we are just at the start of its analysis. We expect to increase our understanding of the fundamental physics of the beautiful phase transition between L and H mode, and finally challenge the various models of the L-H transition, as well as improve predictions for future devices.

References

[1] Wagner F, Becker G., Behringer K., et al., *Phys. Rev. Lett.* 49 (1982) 1408.

[2] ASDEX Team (1989) *Nucl. Fusion* 29 1959

[3] Righi E. et al *Nucl. Fusion* 39 309 (1999)

[4] Maggi C.F. et al (2014) Nucl. Fusion54 023007

[5] E.R. Solano *et al* (2021) *Nucl. Fusion* **61** 124001

[6] Delabie, E. Preprint: *25th IAEA Fusion Energy Conference, Saint Petersburg, Russia, EX-P5/24* (2014).

[7] Solano E.R. *et al* (2022) *Nucl. Fusion* **62** 076026

[8] Hillesheim J. et al, 44th EPS Conf. on Plasma Physics (Belfast, June 2017) P5.162

[9] Maggi C.F. et al., *Plasma Phys. Control. Fusion* 60 (2018) 014045

[10] Birkenmeier G. *et al* (2022) *Nucl. Fusion* **62** 086005

[11] Birkenmeier G. el al, 1st revision submitted to PPCF, PPCF-104045.R1, likely to be published in 2023.

[12] Schissel D. P. et al., in Controlled Fusion and Plasma Physics (Proc. 16th Eur. Conf. Venice, 1989), Vol. 13B, Part I, European Physical Society, Geneva (1989) 115.

[13] Osborne T.H. *et al* 1990 *Nucl. Fusion* **30** (2023) **DOI** 10.1088/0029-5515/30/10/004

[14] Ryter, F., et al., in Controlled Fusion and Plasma Physics (Proc. 20th Eur. Conf. Lisbon, 1993), Vol. 17C, Part I, Euro- pean Physical Society, Geneva (1993) 23.

[15] Lebedev S V *et al* (1994) *Plasma Phys. Control. Fusion* **36** B289

[16] Snipes J.A. *et al* (1994) *Nucl. Fusion* **34** 1039

[17] Gao Xiang *et al* (1994) *Chinese Phys. Lett.* **11** 161

[18] Fielding S.J., et al, Journal of Nuclear Materials,Volumes 220–222 (1995) Pages 284-287, https://doi.org/10.1016/0022-3115(94)00429-3.

[19] Kardaun, O. J. W. F., F. Ryter, and U. Stroth, *Plasma physics and controlled nuclear fusion research 1992. V. 3.* (1993).

[20] Thomsen K. et al 1994 *Nucl. Fusion* 34 131

[21] Martin Y R et al *J. Phys.: Conf. Ser.* 123 012033 (2008)

[22] Delabie E. et al, 'Status of TC-26: L-H/H-L scaling in the presence of Metallic walls', ITPA meeting September 2017

[23] Ryter F et al (2013) *Nucl. Fusion* 53 113003

[24] ITER Organisation (2018) *ITER Research Plan within the Staged Approach ITR-18-003* p 351

[25] Horton L. et al, Fusion Engineering and Design 109–111 (2016) 925–936

[26] Carvalho I. et al. *Fusion Engineering and Design* 124: 841–45 (2017) https://doi.org/10.1016/j.fusengdes.2017.03.069

[27] Vartanian S. *et al* (2021) *Fusion Eng. Des.* **170** 112511

[28] Hawkes N. C., Rev. Sci. Inst. 89, 10D113 (2018); https://doi.org/10.1063/1.5037639

[29] Lennholm M., et al, *Fusion Engineering and Design* 48 (1–2): 37–45 (2000). https://doi.org/10.1016/S0920-3796(00)00125-3.

[30] Solano E. R et al, 46th EPS Conference on Plasma Physics, 8-12 July 2019, poster P5.1081 http://ocs.ciemat.es/EPS2019PAP/pdf/P5.1081.pdf

[31] Greenwald M. *et al* (1988) *Nucl. Fusion* **28** 2199

[32] Solano E. R. *et al* (2017) *Nucl. Fusion* **57** 022021

[33] Silva C et al Nuclear Fusion 61 (12), 126006 (2021)

[34] Silva C. *et al* (2022) *Nucl. Fusion* **62** 126057

[35] Gohil P., Nucl. Fusion 51 (2011) 103020

[36] Pawelec E., to be presented at EPS 2023.

[37] F Ryter et al, Nucl. Fusion 54 083003 (2014)

[38] Plank U et al (2023) Plasma Phys. Control. Fusion 65 014001

[39] Vincenzi P et al (2022) Plasma Phys. Control. Fusion 64 124004

[40] Mantsinen, M. et al, submitted to T&DT Nucl. Fus. Special Issue.

[41] Rodriguez-Fernandez, P. et al NF 62 042003 (2022)